


RESEARCH

Open Access



Recycling machinery of integrin coupled with focal adhesion turnover via RAB11-UNC13D-FAK axis for migration of pancreatic cancer cells

Van-Thanh Duong¹, Mihyang Ha², Jayoung Kim³, Ji-Young Kim¹, Siyoung Park¹, Khatun Mst Reshma¹, Myoung-Eun Han¹, Dongjun Lee³, Yun Hak Kim^{1,4} and Sae-Ock Oh^{1*} 

Abstract

Background Recycling of integrin via endosomal vesicles is critical for the migration of cancer cells, which leads to the metastasis of pancreatic cancer and devastating cancer-related death. So, new diagnostic and therapeutic molecules which target the recycling of endosomal vesicles need to be developed.

Methods Public databases including TCGA, ICGC, GSE21501, GSE28735, and GENT are analyzed to derive diagnostic and therapeutic targets. To reveal biological roles and underlying mechanisms of molecular targets, various molecular biological experiments were conducted.

Results First, we identified UNC13D's overexpression in patients with pancreatic cancer (n = 824) and its prognostic significance and high hazard ratio (HR) in four independent pancreatic cancer cohorts (TCGA, n = 178, p = 0.014, HR = 3.629; ICGC, n = 91, p = 0.000, HR = 4.362; GSE21501, n = 102, p = 0.002, HR = 2.339; GSE28735, n = 45, p = 0.022, HR = 2.681). Additionally, its expression is associated with the clinicopathological progression of pancreatic cancer. Further biological studies have shown that UNC13D regulates the migration of pancreatic cancer cells by coupling the exocytosis of recycling endosomes with focal adhesion turnover via the regulation of FAK phosphorylation. Immunoprecipitation and immunocytochemistry showed the formation of the RAB11-UNC13D-FAK axis in endosomes during integrin recycling. We observed that UNC13D directly interacted with the FERM domain of FAK and regulated FAK phosphorylation in a calcium-dependent manner. Finally, we found co-expression of UNC13D and FAK showed the poorest survival (TCGA, p = 0.000; ICGC, p = 0.036; GSE28735, p = 0.006).

Conclusions We highlight that UNC13D, a novel prognostic factor, promotes pancreatic cancer progression by coupling integrin recycling with focal adhesion turnover via the RAB11-UNC13D-FAK axis for the migration of pancreatic cancer cells.

Keywords UNC13D, RAB11, FAK, Integrin, Focal adhesion, Migration, Prognosis, Pancreatic cancer

*Correspondence:

Sae-Ock Oh

hedgehog@pusan.ac.kr

Full list of author information is available at the end of the article



© The Author(s) 2024. **Open Access** This article is licensed under a Creative Commons Attribution-NonCommercial-NoDerivatives 4.0 International License, which permits any non-commercial use, sharing, distribution and reproduction in any medium or format, as long as you give appropriate credit to the original author(s) and the source, provide a link to the Creative Commons licence, and indicate if you modified the licensed material. You do not have permission under this licence to share adapted material derived from this article or parts of it. The images or other third party material in this article are included in the article's Creative Commons licence, unless indicated otherwise in a credit line to the material. If material is not included in the article's Creative Commons licence and your intended use is not permitted by statutory regulation or exceeds the permitted use, you will need to obtain permission directly from the copyright holder. To view a copy of this licence, visit <http://creativecommons.org/licenses/by-nc-nd/4.0/>.

Background

The trafficking of endosomal vesicles is critical for the migration and invasion of cancer cells by recycling cell surface cargos, including growth factors and adhesion receptors [1]. This recycling of surface cargo enables cancer cells to increase the number of growth factors and adhesion receptors, prompting the amplification of mitogenic and motogenic stimulations. Endocytosed cargo from the cell surface is delivered to the early endosome for recycling back to the cell surface or for targeted degradation. The sorting of vesicles for recycling or degradation is regulated by the endosomal sorting complex required for transport (ESCRT) or distinct molecular assemblies such as the retromer/SNX27/WASH, retriever, and FERARI complexes. In these processes, endosomes can play the role of an important signaling platform. For example, active integrins and pFAK in early endosome contribute to the suppression of anoikis and anchorage-independent growth [2]. Moreover, endosomal recycling of c-Met is critical for the activation of Rac and cytoskeleton signaling for the migration and invasion of cancer cells. However, during the endosomal recycling processes, how the signaling activity is regulated remains poorly characterized.

Recycling of surface cargo occurs mostly through Rab4- and Rab11-dependent routes, which are antagonistic to each other [3]. The Rab4 route is associated with fast recycling of $\alpha\beta3$ integrin and Rac-mediated slow and persistent migration [1]. The Rab11 route with the slow recycling of $\alpha\beta1$ and RhoA-mediated rapid migration. The Rab11 pathway is involved in perinuclear endosomal recycling Rab11 induces the production of recycled endosomes from early endosomes after activation by PtdIns (3P), which is produced by PI3KC2A. After the production of recycled vesicles from early endosomes, they contribute to the tethering, docking, and fusion of vesicles to the plasma membrane. For the docking of Rab11-positive vesicles to the plasma membrane, UNC13D is required as its effector molecule [4].

The main biological role of UNC13D has been documented in immune cells, in the secretion of lysosomes to immunological synapses [5]. Mutations in UNC13D cause defects in lysosomal secretion, leading to impaired lymphocyte cytotoxicity and the development of familial hemophagocytic lymphohistiocytosis type 3, an immunodeficiency disorder. UNC13D, together with Rab27a and PI(4,5)P₂, is important for the tethering of secretory lysosomes to the plasma membrane, which increases the dwelling time of secretory lysosomes at the immunological synapse, facilitating the subsequent fusion with the plasma membrane and release of lytic

contents. In addition to its role in immune cells, its critical role in the Rab11-dependent secretion of cancer cell exosomes has been documented in pancreatic cancer cells [6].

Coordinated assembly and disassembly of focal adhesions (FAs) at the leading and rear edges are critical for the migration of cancer cells [7, 8]. The assembly of FAs begins with the clustering of integrins and is stabilized by linking to actin stress fibers via Rho/ROCK. Its disassembly is triggered by the extension of microtubules and the endocytosis of integrins. During assembly of FA, integrins at the plasma membrane interact with the extracellular matrix and recruit many cytosolic proteins including talin, vinculin, paxillin, alpha-actinin, and focal adhesion kinase (FAK) [7]. The disassembly of FAs is conducted via dynamin-dependent endocytosis, and surface integrins are endocytosed and transported to early endosomes. FAK is critical for various steps of FA recycling. Its binding to Grb2 recruits dynamin to FAs and initiates integrin internalization. Therefore, FAK deficiency impairs the disassembly of FA [9].

FAK is a critical protein for the progression of cancer by regulating proliferation, apoptosis, survival, migration, and stemness of cancer cells [10, 11]. It is composed of three main domains: a four-point-one-ezrin-radixin-moesin (FERM) domain, a kinase domain, and a C-terminal focal adhesion targeting (FAT) domain. The FERM domain contains a nuclear localization sequence and regulates p53 ubiquitination and degradation via the interaction with E3 ligases [12]. This domain also prevents FAK activation by the inhibitory interaction with the kinase domain [13]. So, it is a hot regulatory target site for FAK activation via the interaction with various molecules including integrin and growth factor receptors [14, 15]. The FAT domain is important for the recruitment and activation of FAK at FAs. There are at least six tyrosine residues which can be phosphorylated. Y397 is the sole autophosphorylation site and provides a binding site for Src kinases and other proteins containing the SH2 domain. The phosphorylation of Y925 can recruit Grb2 and increase the activity of Ras/MAPK signaling [16]. FAK is critical not only for the assembly of focal adhesion complexes but also for its disassembly. It can regulate the disassembly of focal adhesion complex by increasing Grb2-MAPK-Myosin light chain kinase (MLCK) pathway [17] or by suppressing Rho activity [18, 19].

Pancreatic cancer is one of the most aggressive types of malignant tumors and the fourth leading cause of cancer-related deaths worldwide [20]. Despite the development of surgical techniques and systemic treatments, owing to local invasiveness and metastasis to distant organs

at an early stage, the outcome of pancreatic cancer remains disappointing, with an average five-year survival rate of approximately 10% [20, 21]. While searching for prognostic factors for pancreatic cancer, we observed that UNC13D was a novel prognostic factor in four independent cohorts and promoted the migration of cancer cells by direct interaction with FAK for the coupling of the endosomal recycling machinery with FA turnover.

Methods

Public data sources and statistical analysis

To analyze UNC13D expression in tissues from healthy adult humans and cancer patients, primary and processed data were downloaded from GSE28735, TCGA, GTEx, and GENT. To correlate UNC13D expression with clinicopathological characteristics, mRNA expression and clinical data were obtained from the TCGA database. For the analysis of prognostic value, TCGA, ICGC, GSE21501, and GSE28735 datasets were downloaded. The following samples were excluded: (1) those with “0” gene expression values and (2) those with insufficient clinicopathological and survival information. These analyses were performed in R, using the “cgdsr” and “GEOquery” packages. The Wilcoxon signed rank test was performed for the comparison of UNC13D expression values between paired cancer and normal pancreatic samples using the “coin” R package. The Mann–Whitney U test or Student’s T-test was used to determine the significance of differences between the mean values of two unpaired groups. For comparison of more than three groups, one-way analysis of variance (ANOVA) followed by Tukey’s multiple comparisons test or the Kruskal–Wallis test by rank was used. The correlation between UNC13D and clinicopathological characteristics was evaluated using the Chi-squared test. All statistical analyses were performed using the R software version 4.2.0 (<https://www.R-project.org/>), and statistical significance was set at p value < 0.05.

Cell culture

Human PC cell lines (PANC-1, MIA PaCa-2, AsPC-1, CAPAN-1, and SNU213) and human embryonic kidney 293 (HEK293) cell lines were obtained from the American Type Culture Collection (ATCC). The cell lines were cultured in DMEM supplemented with 10% fetal bovine serum and 1% penicillin or streptomycin or RPMI-1640 containing 10% fetal bovine serum, 1% penicillin or streptomycin, and 25 mM HEPES under conditions of 5% CO₂ and 37 °C in a humidified environment. All cell lines were authenticated by short tandem repeat profiling and tested for mycoplasma contamination.

Expression vectors and Mutagenesis

The pcDNA3.1-FAK-HA and pcDNA3.1-FAK-HA domain plasmids were kindly provided by Prof. Min Do Sik (Department of Pharmacy, Yonsei University, Korea). The plasmid p3xFLAG-CMV10-UNC13D was obtained from transOmic Tech. The pEGFP-FAK (#50,515), pKAR1/PUR (#23,105), mCerulean3-C1 (#54,605), and mCerulean-Rab11a-7 (#55,390) were purchased from Addgene (Cambridge, MA, USA). FLAG- or HA-tagged UNC13D and its truncation mutants, HA-tagged FAK, and some of its truncation mutants were constructed using standard molecular biology techniques. All constructs and mutations were confirmed using nucleotide sequencing analyses (Cosmogenetech).

Transfection and stable cell line construction

AsPC-1, MIA PaCa-2, CAPAN-1, and PANC-1 cells were transfected with siRNA or cDNA constructs using DharmaFECT1 (Thermo Scientific, Lafayette, CO, USA) or Lipofectamine 3000 (Cat #L3000075, Thermo Fisher Scientific, Lafayette, CO, USA). For siRNA transfection, scrambled (SCR) and UNC13D siRNAs were purchased from Dharmacon (Lafayette, CO, USA) and Bioneer Corporation (Daejeon, Korea), respectively. The siRNA sequences used were as follows: siSCR, 5'- UUU CGC UCU UUU GCG GAU G(dTdT) -3' and 5'-GAU CCG CAA AAG AGC GAA A(dTdT) -3'; and UNC13D siRNA, for coding sequence targeting (CDS). 5'- CAC AUC AGC GGU GGA UCU A(dTdT) -3' and 5'- UAG AUC CAC CGC UGA UGU G(dTdT) -3'; 5'-CAU GAU UAC CGU CAA GUU U(dTdT) -3' and 5'-AAA CUU GAC GGU AAU CAU G- (dTdT) -3'; 5'- GUC AUC ACC CAG ACA CUC A(dTdT) -3' and 5'-UGA GUG UCU GGG UGA UGA C(dTdT) -3'. To generate stable knockdown cell lines, CAPAN-1 cells were transfected with shSCR or shUNC13D expression constructs pKAR1/PUR (Addgene, Cat No. #23,105) using Lipofectamine 3000 reagent. Transfected cells were selected using puromycin (Sigma-Aldrich, St. Louis, MO, USA) 0.3 µg/ml for four weeks, and the knockdown efficiency was assessed by real-time PCR and western blotting.

Antibodies and reagents

The antibodies and dilutions used in this study included an anti-UNC13D antibody (16905–1-AP, 1:1000) purchased from Proteintech (Chicago, USA). Anti-HA (ab9110, 1:2000) and anti-integrin beta1 (12G10, ab30394, 1:500) were purchased from Abcam (Cambridge, UK). Anti-FAK (3285, 1:2000), anti-phosphorylated FAK (Y397, 3283, 1:2000), anti-phosphorylated FAK (Y576/577, 3281, 1:2000), anti-Erk1/2 (9102, 1:2000), anti-phosphorylated Erk1/2 (9101, 1:2000), anti-phosphorylated Src (Y416, 6943,

1:2000), and anti-Src antibodies (2109, 1:2000) were purchased from Cell Signaling Technology (Beverly, MA, USA). Anti-phosphorylated paxillin antibodies (Y118, 44-722G, 1:4000) and anti-phosphorylated FAK antibodies (Y861, 44-626G, 1:2000) were purchased from Invitrogen (Gaithersburg, MD, USA). Anti-Rab11A (A-6, sc-166912, 1:200) and anti- β -actin antibodies (C4, sc-47778, 1:5000) were purchased from Santa Cruz (CA, USA). Anti-paxillin (610051, 1:10,000), anti-integrin beta1 (mAb13, 552828, 1:200), and anti-Rab11 antibodies (610656, 1:2000) were purchased from BD Biosciences (NJ, USA). Anti-FLAG (M2, F3165; 1:5000) and anti-HA (HA-7, H9658; 1:2000) antibodies were purchased from Sigma-Aldrich (St Louis, MO, USA). Phalloidins (A12381, 1:100), DAPI (D1306, 1:500), Protein A dynabeads (10002D), Protein G dynabeads (10004D), and Lipofectamin 3000 (L3000015) were purchased from Invitrogen (Gaithersburg, MD, USA). Ionomycin (56092-82-1), EGTA (E3889), and nocodazole (SML1665) were purchased from Sigma-Aldrich (St Louis, MO, USA). Dharmafect 1 (T-2001-02) was purchased from Thermo Scientific (Dharmacon, Lafayette, CO, USA). FAK inhibitor VS-4718 (S7653) was purchased from Selleckchem (Texas, USA). Primary antibodies and reagents are summarized in Supplementary Table 1.

Real-time PCR

Total RNA was isolated using an RNeasy Mini Kit (Qiagen, Valencia, CA, USA) according to the manufacturer's instructions. Reverse transcription was performed using oligo-dT, dNTP, RNasin, and MMLV reverse transcriptases (Promega). Quantitative real-time PCR (qRT-PCR) was completed with SYBR green PCR Master Mix on an ABI QuantStudio 3 Detection System (Applied Biosystems, USA) to determine UNC13D, RAB11a mRNA levels, and relative quantification of mRNA levels were calculated by the comparative Ct method ($2^{-\Delta\Delta Ct}$). The primers for qRT-PCR were as follows: GAPDH forward primer 5'- GAG TCC ACT GGC TTC AC -3'; GAPDH reverse primer 5'- ATG ACG AAC ATG GGG GCA TC -3'; UNC13D forward primer 5'- GCA CAT CAG CGG TGG ATC TAT -3'; UNC13D reverse primer 5'- AGG TGT CCT CCA CAA ACT TGA C -3'; RAB11A forward primer 5'- ACG TCA TCT CAG GGC AGT TC -3'; and RAB11A reverse primer 5'- TGT AGA GTC TAG GGC CGA AGT -3'. Primer information is summarized in Supplementary Table 1.

Immunoblotting

Immunoblot analysis was performed as previously described [22]. Briefly, cell lysates were prepared using RIPA buffer (50 mM Tris-HCl [pH 8.0], 1% Nonidet

P-40, 0.5% sodium deoxycholate, 0.1% SDS, and 150 mM NaCl) containing a protease inhibitor cocktail (Roche, Basel, Switzerland). The whole lysed fraction was sonicated on ice to avoid heat and air bubbles and subsequently centrifuged for 20 min at 15,000 \times g. Protein concentration was determined using the BCA assay (Intron), and proteins were denatured in a sample buffer immediately before SDS-PAGE. Subsequently, 15 to 30 μ g of cell lysates were applied to SDS-PAGE electrophoresis and transferred to polyvinylidene fluoride (PVDF) membranes by a wet-transfer system (BioRad). After blocking in TBST buffer containing 5% skim milk for 1 h at room temperature, subsequently probed with individual primary antibodies overnight at 4 °C. The following day, blots were incubated with either anti-mouse or anti-rabbit IgG conjugated to horseradish peroxidase (Promega). Immunoblots were visualized using a chemiluminescence Imaging System (GE Healthcare, Cambridge, UK). For confirmation of the amounts of loaded samples, the membranes were incubated with an anti- β -actin-HRP antibody overnight at 4 °C. The densitometric analysis of the blots was calculated as a ratio of target protein versus β -actin using ImageJ. Quantitative graphs were analyzed using the Prism 8 software.

Immunocytochemistry (ICC)

ICC experiments were performed as previously described by Tran et al. [23]. Briefly, cells were seeded and grown on an 8-well Chamber Slide and fixed with 4.0% paraformaldehyde for 15 min at RT. After washing with PBS, fixed cells were permeabilized with 0.1% Triton X-100 in PBS for 10 min. Nonspecific binding was blocked in 3% BSA in PBS for at least 1 h. The cells were then stained with the indicated primary antibodies diluted in blocking solution overnight at 4 °C, rinsed three times with PBS, incubated with secondary antibodies (Alexa488- or Alexa594-conjugated) in blocking buffer for 1 h at room temperature, washed with PBS for three times, and then counterstained with 4', 6-diamidino-2-phenylindole (DAPI; Sigma-Aldrich) for 10 min at room temperature. The slides were mounted and observed under a confocal laser-scanning microscope (LSM 900; Zeiss Microscopy GmbH).

Co-immunoprecipitation (Co-IP) assay

Co-IP experiments were performed as described by Tran et al. [23]. Briefly, Co-IP experiments were performed by incubating individual antibodies with 0.2–1 mg of whole cell lysates prepared by pierce IP lysis buffer in 25 mM Tris-HCl pH 7.4, 150 mM NaCl, 1% NP-40, 1 mM EDTA, 5% glycerol, 1 mM PMSE, and protease inhibitors. The immune complexes were incubated overnight at 4 °C,

supplemented with protein- A or protein- G Dynabeads (Life Technologies Corporation), and then incubated for 2 h at 4 °C. The Dynabeads-Ab complexes were washed three times with the same lysis buffer, dissolved in 2X sample buffer containing 30 mM Tris-HCl (pH 6.8), 12.5% glycerol, 1% SDS, 7.2 mM 2- mercaptoethanol, and 0.1% bromophenol blue, denatured at 95 °C for 5 min, and then separated by SDS-PAGE. After transfer, the membranes were blocked with 5% skim milk, incubated with different primary antibodies overnight, and then incubated with secondary antibodies sequentially and developed.

Cell proliferation assay

The proliferation of pancreatic cancer cells was assessed using an Ez-Cytox proliferation assay kit (ITSBIO, Seoul). Briefly, 3–5 days after SCR or UNC13D siRNA transfection, 10 µl of Ez-Cytox was added into each well and incubated for 1–2 h in a CO₂ incubator. Optical density (OD) was measured at 450 nm using an ELISA reader (Tecan, Mannedorf, Switzerland). SCR siRNA was used as a control to determine relative cell proliferation.

Boyden chamber assay

A modified Boyden transwell chamber (Unk Probe, Gaithersburg, MD, USA) was used. FBS-induced cell migration was examined two days after SCR or UNC13D siRNA transfection. Culture medium (50 µl of culture medium containing 10% FBS) was added to the bottom chambers, which were covered with collagen-coated membranes. Cells were diluted in a culture medium containing 0.25 µg/mL of mitomycin C. Next, 2.5×10^4 cells (50 µl) were added to the upper chambers. After 24 h, the cells on the upper surface were removed by wiping with cotton swabs, and the cells that had migrated through the membrane on the lower surface were fixed and stained using Diff-Quik solution (38,721, Sysmex, Kobe, Japan). The total number of migrated cells was captured using a light microscope (Olympus BX50) and counted using the Adobe Photoshop CS6 software (RRID: SCR_014199). The results were normalized using the results of SCR siRNA controls.

Wound healing assay

SCR or UNC13D siRNA-transfected cells were seeded at 2×10^5 cells per well in 24-well plates. Cells were cultured to 90% confluence, and scratched using a 200 µl pipette tip, washed twice with 1X PBS, and then fresh medium containing 0.25 µg/mL of mitomycin C and 0.1% FBS was added. Images were acquired immediately and at 0, 12, and 24 h after scratching. For quantification, scratch widths were measured using ImageJ software (version

8; National Institutes of Health). The results were normalized to those of the SCR siRNA controls.

Matrigel invasion assay

To investigate FBS-induced cell invasion, we used 24 well cell culture inserts (353,097; Corning Life Sciences, Glendale, AZ, USA) were used. The upper surfaces of the inserts were covered with 30 µl of 0.5 mg/mL of growth factor-reduced Matrigel (356230, Corning Life Sciences), and the lower surfaces of the inserts were covered with 20 µl of 0.5 mg/mL fibronectin (356008, Corning Life Sciences). The coated inserts were rehydrated with culture medium for 4 h in a CO₂ incubator. Within one to two days of SCR or UNC13D siRNA transfection, 5×10^4 cells in 500 µl of media containing 0.1% FBS were added to the inserts. To observe chemotactic cell invasion, 700 µl of the culture medium containing 10% FBS was added to each well. Mitomycin C (10107409001, 0.25 µg/ml; Sigma-Aldrich) was used to inhibit the proliferation of MiaPaca-2 and PANC-1 cells. After incubation for 48 h, cells on the upper surfaces of the inserts were removed by scraping. The cells that penetrated the inserts were fixed and stained using a Diff-Quik solution (Sysmex, Kobe, Japan). The total number of invading cells was captured using a light microscope (Olympus microscope SZX7) and counted using Adobe Photoshop CS6 software (RRID: SCR_014199).

FA dynamics analysis

This assay was performed as previously described by Ezratty et al. [9]. To analyze the dynamics of FAs (FA disassembly/nocodazole washout assay), cells were grown on 8-well chamber slides, starved overnight in a medium containing 0.1% serum, and incubated with 10 mM nocodazole (SML1665, Sigma-Aldrich) in serum-free medium for 4 h to depolymerize microtubules (MTs), as previously described [9]. The drug was washed with a serum-free medium to allow MTs reformation, and the cells were incubated at 37 °C for different time points (0, 30, and 60 min). The cells were then fixed using 4% formaldehyde for 15–20 min and stained with an anti-paxillin antibody. FA disassembly was analyzed by manually counting the punctate and elongated structures that were positive for paxillin. The number of FAs was normalized to the number of cells analyzed. Data were normalized to the number of FAs in the control cells. FA disassembly rate was calculated as follow: $\text{FA disassembly} = \frac{\text{number of disassembled FAs}}{\text{total number of FAs}} * 100 = \frac{\text{FAs at 0 min} - \text{FAs at 60 min}}{\text{FAs at 0 min}} * 100$. To assess FA levels in western blots (Fig. 2F), transfected CAPAN-1 cells were grown on 60 mm plates, starved in serum-free medium for 12 h, and then the protocol described above was followed.

Whole-cell extracts were subjected to SDS-Page, and incubated overnight at 4 °C with p-FAK (Y397) or total FAK. The following day, membranes were incubated with secondary antibodies and developed.

Quantification and statistical analysis for the analysis of biological experiments

All fluorescence images were analyzed using Zen imaging software (Zeiss), and the background was quantified by subtraction using ImageJ software (RRID: SCR_003070). All statistical analyses of biological experiments were performed using the GraphPad Prism 8 software (GraphPad, San Diego, USA). Three or more mean values were compared using a one-way analysis of variance (ANOVA), whereas two comparisons were performed using an unpaired Student's *t*-test. Quantitative data were presented as mean ± S.D. of at least three pooled experiments, and the significance was indicated in the legend of each figure.

Data availability statement

Derived data supporting the findings of this study and materials are available from the corresponding author [SO Oh] on request.

Results

Overexpression of UNC13D and its association with clinicopathologic characteristics in pancreatic cancer patients

To evaluate the expression status of UNC13D in pancreatic cancer, we compared its expression in cancerous and matched normal pancreatic tissues using the GSE28735 data (n=45). UNC13D expression was significantly higher in cancer tissues than in matched normal tissues (Fig. 1A; Wilcoxon signed-rank test). Although normal tissues did not match their cancer tissues, we compared their expression levels using GTEx and TCGA (n=350) cohorts and observed consistent results (Fig. 1B, Student T test). To further expand the patient cohort, we analyzed the GENT database, which contains various GEO data. Pancreatic cancer tissues in the GENT database (n=429) showed overexpression of UNC13D compared to normal tissues (Fig. 1C, Student

T test). Collectively, the data from 824 patients showed overexpression compared with normal tissues.

To evaluate the association of UNC13D with the clinicopathological characteristics of pancreatic cancer patients, we examined the information of 178 patients from the TCGA cohort. Patient information used in this study is listed in Table 1. Note that high UNC13D expression was associated with high pathological grade ($p=0.001$, chi-squared test, Table 1), late TNM stage ($p=0.000$, chi-squared test, Table 1), and late T stage ($p=0.003$, chi-squared test, Table 1). Accordingly, the expression levels of UNC13D tended to increase (Fig. 1D) with the progression of pathological grades ($p=0.002$, Kruskal–Wallis test), TNM stage ($p=0.021$, Student T test), and T stage ($p=0.041$, Student T test).

Prognostic significance of UNC13D in pancreatic cancer patients

Next, we examined whether UNC13D overexpression is associated with patient prognosis. To evaluate prognostic significance, we performed Kaplan–Meier curve analysis for survival with respect to UNC13D gene expression. We examined the data of 416 patients from four independent cohorts (TCGA, n=178; ICGC, n=91; GSE21501, n=102; and GSE28735, n=45). Note that higher expression of UNC13D showed shorter survival rates in TCGA, ICGC, GSE21501, and GSE28735 cohorts ($p=0.011$, $p=0.009$, $p=0.035$, and $p=0.006$, respectively; Fig. 1E). Moreover, its prognostic significance was evaluated using the Cox regression analysis. Univariate analysis showed significance in all four cohorts (TCGA, $p=0.014$, HR=3.629; ICGC, $p=0.000$, HR=4.362; GSE21501, $p=0.002$, HR=2.339; and GSE28735, $p=0.022$, HR=2,681, Table 2). Furthermore, multivariate analysis showed consistent results (TCGA, $p=0.031$; ICGC, $p=0.000$; and GSE21501, $p=0.008$, Table 2). The UNC13D hazard ratio (HR) was particularly high compared to other factors (TCGA, HR=3.120; ICGC, HR=6.488; and GSE21501, HR=2.131, Table 2).

(See figure on next page.)

Fig. 1 Expression level and prognostic significance of UNC13D and FAK (PTK2) in pancreatic cancer. **A** Comparison between cancer and matched normal pancreas tissue from GSE28735 cohort (n=45, Wilcoxon signed rank test). **B** Comparison between cancer and normal pancreas tissues from TCGA and GTEx cohort (n=350, Mann–Whitney U test). **C** Comparison between cancer and normal pancreas tissues from GEO cohorts in GENT database (n=429, Mann–Whitney U test). **D** Expression level of UNC13D in patients of each subgroup of pancreatic cancer (TCGA, n=178). **E** Kaplan–Meier survival analysis of HCC patients according to the UNC13D and FAK (PTK2) gene expression. Overall survival in TCGA (n=178), ICGC (n=91), GSE21501 (n=102), and GSE28735 (n=45) were examined according to the UNC13D, FAK (PTK2), or both expression (Log-rank test). The *p* value is provided inside each graph

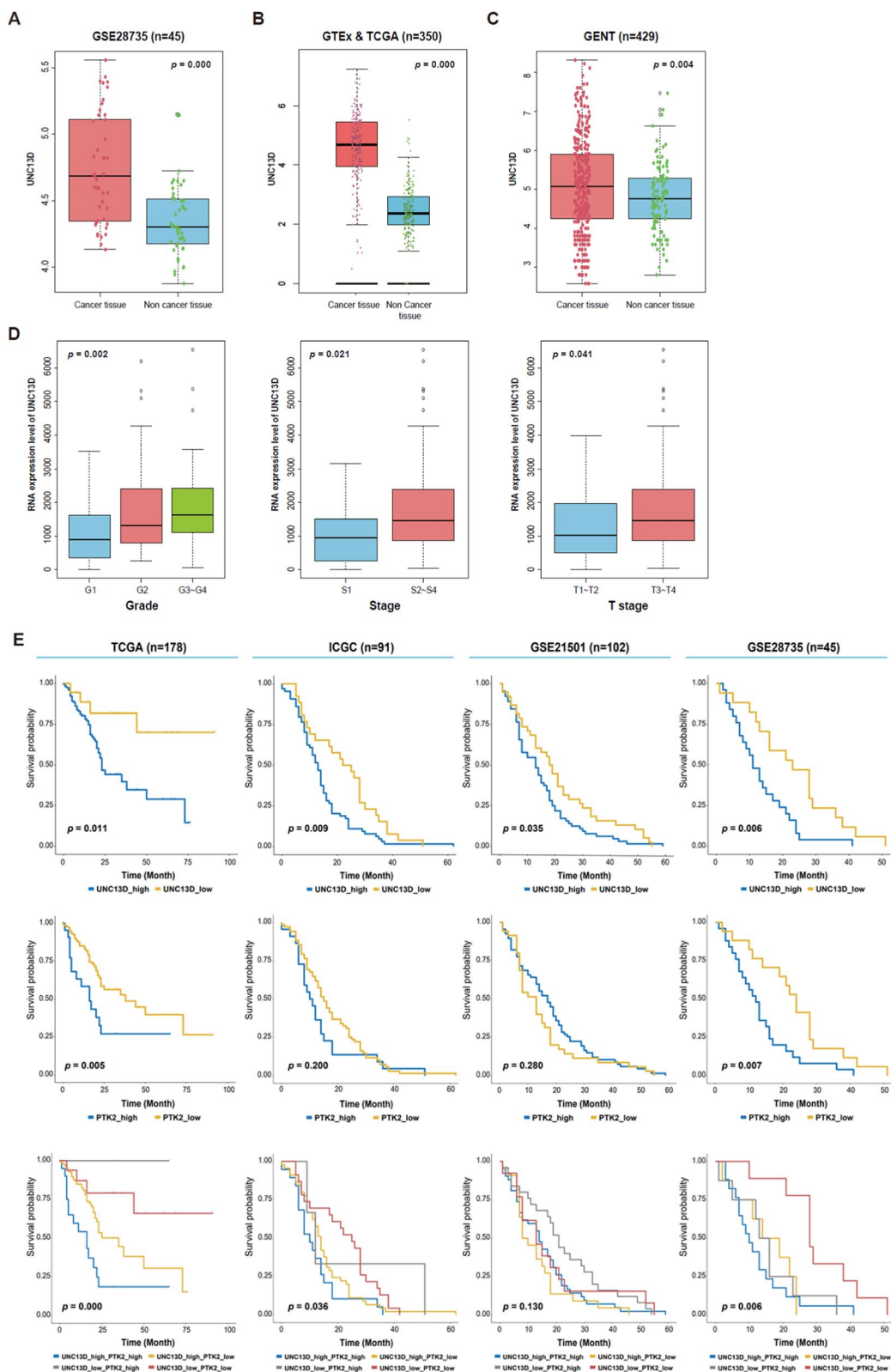


Fig. 1 (See legend on previous page.)

Table 1 Clinicopathological characteristics of patients and their association with UNC13D expression (TCGA, n = 178)

Clinical classification	Expression level of UNC13D case No. (%)			p value
	Total	High (N = 158)	Low (N = 20)	
Age				0.695
≤ 60	55	50 (31.6)	5 (25.0)	
60 <, ≤ 70	57	49 (31.0)	8 (40.0)	
70 <	66	59 (37.3)	7 (35.0)	
Gender				0.637
Male	98	86 (54.4)	12 (60.0)	
Female	80	72 (45.6)	8 (40.0)	
Grade				0.001*
G1	31	22 (14.0)	9 (47.4)	
G2	95	88 (56.1)	7 (36.8)	
G3 & G4	50	47 (29.9)	3 (15.8)	
Stage (TNM)				0.000**
S1	21	13 (8.3)	8 (42.1)	
S2, S3 & S4	155	144 (91.7)	11 (57.9)	
Stage (T)				0.003*
T1 & T2	31	23 (14.6)	8 (42.1)	
T3 & T4	145	134 (85.4)	11 (57.9)	
Stage (M)				0.155
M0	80	75 (96.2)	5 (83.3)	
M1	4	3 (3.8)	1 (16.7)	
Stage (N)				0.071
N0	49	41 (26.3)	8 (47.1)	
N1	124	115 (73.7)	9 (52.9)	

*p value < 0.01, **p value < 0.001

UNC13D regulates the migration and invasion of pancreatic cancer cells via FA turnover

The prognostic significance of UNC13D prompted us to examine its role in the biological behavior of pancreatic cancer cells and related signaling pathways. To determine the functional role of UNC13D in the proliferation of pancreatic cancer cells, we knocked down UNC13D expression using a specific siRNA. Knockdown efficiency was determined using real-time PCR and western blotting (data not shown). Treatment with UNC13D siRNA (siUNC13D) did not affect proliferation (data not shown). Subsequently, we examined the role of UNC13D in the migration and invasion of pancreatic cancer cells. We performed a Boyden chamber assay and siUNC13D suppressed the migration of AsPC-1, PANC-1, CAPAN-1, and SNU213 cells compared to SCR siRNA by 60.6, 63.5, 38.8, and 54.2%, respectively (Fig. 2A, Supplementary Fig. 1). Additionally, siUNC13D significantly reduced the migration of AsPC-1 and PANC-1 cells by 37.5% and 54.8%, respectively, in the wound-healing assay (Fig. 2B). Furthermore, a cell

invasion assay using a Matrigel-coated insert showed that siUNC13D decreased the invasive ability of MiaPACA-2 and PANC-1 cells compared to SCR by 69.6% and 62.8%, respectively (Fig. 2C).

To reveal the underlying mechanisms of UNC13D in regulating the migration and invasion of pancreatic cancer cells, we examined the signaling pathways involved in migration and invasion by analyzing differentially expressed genes depending on the expression level of UNC13D. Differentially expressed genes (DEGs) were identified by comparing RNA expression between UNC13D-high vs -low groups in the TCGA cohort. Gene set enrichment analysis (GSEA, Fig. 2D) showed that UNC13D expression was associated with integrin signaling (NES = 1.75, $p = 0.011$) and FA (NES = 1.63, $p = 0.020$).

Because the analysis of differentially expressed genes revealed the involvement of integrin and FA pathways, we investigated whether UNC13D affects the kinetics of FA disassembly, which are crucial steps in the regulation of cell motility [24]. To this end, we performed immunofluorescence using dual-staining for paxillin (PXN) and F-actin in UNC13D- knockdown cells. PXN, a major component of FAs that serves as a structural adaptor protein connecting the extracellular matrix and cytoskeleton, is dynamic and tends to turnover at the base of newly formed protrusions [25]. The immunofluorescence results showed that compared with the small-sized PXN-containing FAs formed in the control cells, UNC13D-suppressed cells displayed elongated and larger FAs that were predominantly localized in the inner part of the cell body (Supplementary Fig. 2). These data suggested that UNC13D regulates cell migration by regulating FA turnover.

To further investigate whether UNC13D affects FA disassembly, we used a nocodazole washout assay to assess the rate of FA disassembly in a synchronized manner [9]. Briefly, cells were treated with nocodazole, a microtubule-disrupting agent that blocks FA turnover. Nocodazole was then washed out, and the loss of FAs correlated with reduced p-FAK (Tyr397). The more rapid loss of p-FAK (Y397) reflected more rapid FA disassembly. CAPAN-1 stable cells treated with control shRNA (shSCR) or shRNA targeting UNC13D were treated with nocodazole, released for 0, 30, 60 min, and then stained with anti-PXN. After nocodazole washout, shSCR control cells showed a more rapid loss of PXN, where the signals almost disappeared at 60 min, compared to shUNC13D cells (Fig. 2E). Additionally, we monitored p-FAK (Y397) levels by immunoblotting and confirmed that UNC13D knockdown cells had higher basal levels of p-FAK (Y397) than shRNA control cells (Fig. 2F) at approximately 60 min after washout. These

Table 2 The Cox regression analysis of four independent cohorts depending on the expression levels of UNC13D and FAK (PTK2)

Univariate analysis				Multivariate analysis				
Parameters	<i>p</i> *	HR	95 CI	<i>p</i> *	HR	95 CI		
<i>TCGA (n = 178)</i>								
UNC13D	0.014*	3.629	1.293	10.190	0.031*	3.120	1.111	8.762
PTK2	0.006**	2.299	1.276	4.142	0.003**	2.487	1.371	4.513
Age	0.079	1.336	0.968	1.846	0.101	1.309	0.949	1.805
Stage (S1&S2/S3&S4)	0.459	0.474	0.065	3.430	0.516	0.518	0.071	3.775
<i>ICGC (n = 91)</i>								
UNC13D	0.000***	4.362	2.034	9.351	0.000***	6.488	2.564	16.413
PTK2	0.012*	2.043	1.169	3.571	0.872	1.059	0.526	2.132
Age	0.875	0.972	0.686	1.378	0.325	1.212	0.827	1.777
Gender	0.421	0.806	0.477	1.363	0.113	0.582	0.298	1.136
Grade (G1&G2/ G3&G4)	0.011*	2.094	1.186	3.697	0.165	1.556	0.833	2.905
Stage (S1/S2/S3/S4)	0.005**	1.698	1.175	2.455	0.000***	2.097	1.363	3.226
<i>GSE21501 (n = 102)</i>								
UNC13D	0.002**	2.339	1.350	4.054	0.008**	2.131	1.219	3.728
PTK2	0.066	0.627	0.381	1.032	0.009**	0.488	0.284	0.836
T Stage (T1&T2/T3&T4)	0.864	0.948	0.514	1.749	0.262	0.697	0.371	1.309
N Stage (N0/N1)	0.031*	1.863	1.059	3.278	0.015*	2.202	1.169	4.147
<i>GSE28735 (n = 45)</i>								
UNC13D	0.022*	2.681	1.154	6.229	0.112	2.023	0.848	4.825
PTK2	0.014*	2.890	1.241	6.727	0.064	2.305	0.953	5.578

p* value < 0.05, *p* value < 0.01, ****p* value < 0.001

(See figure on next page.)

Fig. 2 UNC13D regulates the migration of pancreatic cancer cells via focal adhesion (FA) turnover. **A, B** Boyden chamber and wound healing assay of cell migration capacity upon UNC13D knockdown in ASPC-1 and PANC-1. Data are presented as the mean ± SD. Two-tailed unpaired Student T test: ***p* < 0.01 and ****p* < 0.001. The quantification data shown are representative of three independent experiments. **C** Analysis of cell invasion capacity upon UNC13D knockdown in MIA PaCa-2 and PANC-1 cells. The quantification data are presented as the mean ± SD of three independent experiments. Two-tailed unpaired Student T test: ***p* < 0.01. **D** Gene set enrichment assay (GSEA) of differentially expressed genes (DEGs) between UNC13D-high vs -low groups in the TCGA cohort indicates the enrichment of the integrin pathway and FA pathway. **E** FA disassembly assay using nocodazole (NDZ) shows UNC13D regulates FA turnover of pancreatic cancer cells. UNC13D knockdown slows FA disassembly. CAPAN-1 shSCR or shUNC13D were starved, left untreated or incubated with 10 μM nocodazole. After 4 h, nocodazole was washed out at different times to allow microtubule regrowth to trigger FA disassembly. The cells were then fixed and immunostained with anti-PXN antibody. Quantification of FAs number was obtained from an average of ten cells of each condition from three independent experiments. Data were shown as mean ± SD of three independent experiments. Two-tailed unpaired Student T test: **p* < 0.05. Scale bar, 10 μm. **F** FAK autophosphorylation and its total form were evaluated by western blot at different times of nocodazole washed-out as in **E**. FAK autophosphorylation was quantified and normalized to total FAK expression

results suggested that UNC13D promotes pancreatic cancer cell migration by accelerating FA disassembly.

UNC13D directly binds with FAK and RAB11 to form RAB11-UNC13D-FAK axis in recycling endosomes

Next, we examined the effects of UNC13D on the activity of FAK, a key player in FA turnover. Additionally, FAK-Tyr397 phosphorylation has been implicated in cell migration and metastasis in various cancers [26, 27]. The knockdown of UNC13D significantly reduced

the phosphorylation of FAK and PXN-Y118, which are well-known substrates of the FAK/Src complex (Fig. 3A). Moreover, VS-4718 (500 nM), an inhibitor of FAK, significantly reduced UNC13D-induced cellular migration and invasion (Supplementary Fig. 3). These results suggested that UNC13D regulates the migration of pancreatic cancer cells through the FAK/PXN signaling pathway.

Next, we examined whether the regulation of FAK by UNC13D was direct or indirect using

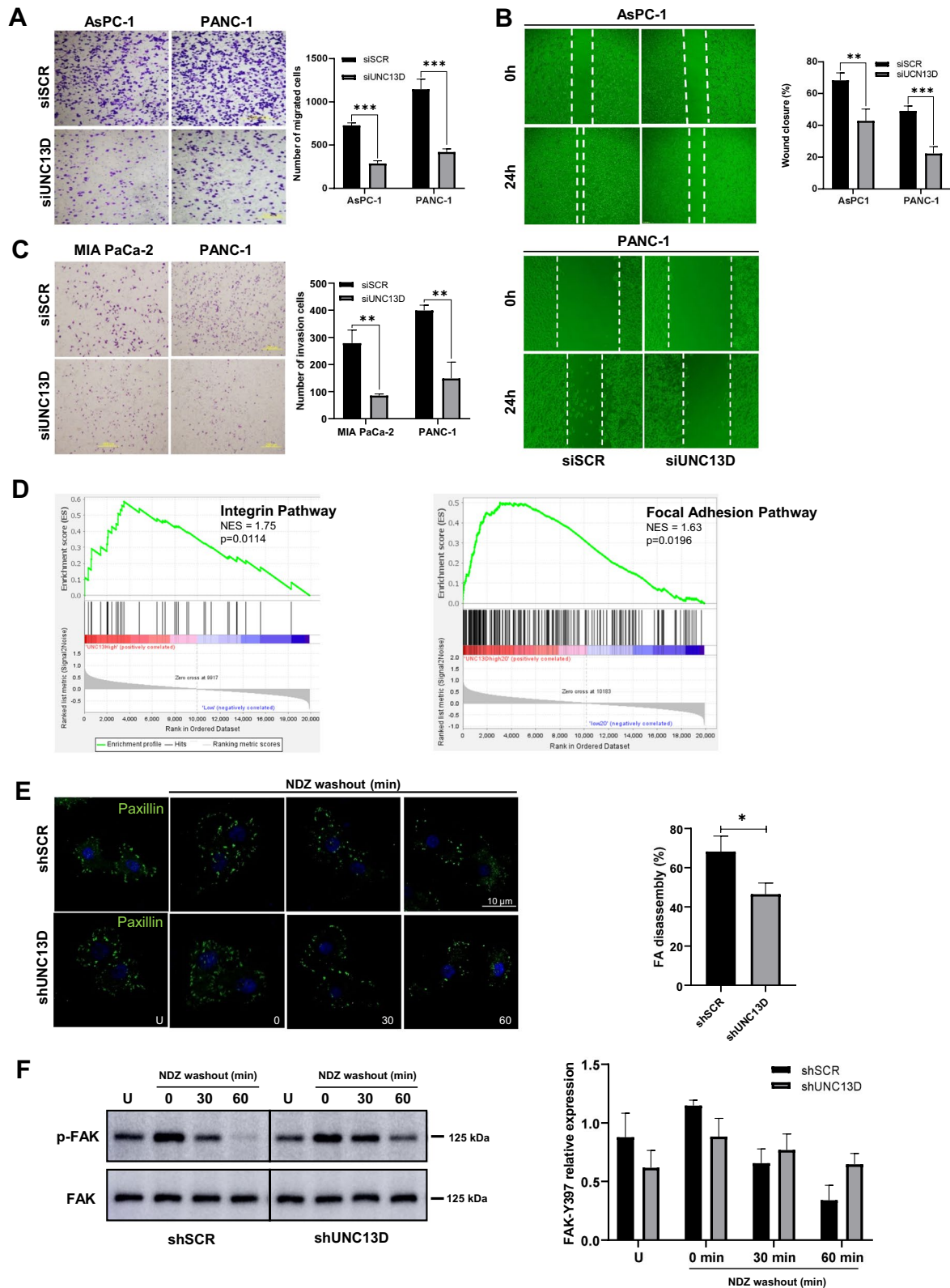


Fig. 2 (See legend on previous page.)

immunoprecipitation. Immunoprecipitation in HEK293 cells after exogenous expression of UNC13D and FAK showed a direct interaction (Fig. 3B). This direct interaction was further confirmed in CAPAN-1 and PANC-1 cells by endogenous immunoprecipitation without exogenous expression (Fig. 3C). These results suggest that UNC13D regulates the FAK/PXN signaling pathway via a direct interaction with FAK.

In contrast to normal cells, cancer cells alter their endocytic trafficking pathway to provide a more efficient supply of materials during migration [26, 28]. UNC13D has been reported to bind to RAB11 for RAB11-positive vesicle trafficking [4] and is critical for driving exosome release [6]. Therefore, co-immunoprecipitation experiments were conducted to examine the interaction between UNC13D and RAB11 in pancreatic cancer cells. Consistent with previous reports, UNC13D was found to interact with endogenous RAB11 in PANC-1 cells (Fig. 3D). We examined the formation of a protein complex comprised of UNC13D-FAK-RAB11. Co-immunoprecipitation results showed that UNC13D and FAK interacted with endogenous RAB11 in PANC-1 cells (Fig. 3E). These results suggest the formation of the RAB11-UNC13D-FAK axis in pancreatic cancer cells.

Next, we examined whether UNC13D was required for the interaction between RAB11 and FAK. siUNC13D reduced the interaction between RAB11 and FAK as examined by immunoprecipitation (Fig. 3F), further confirming the formation of the RAB11-UNC13D-FAK axis.

To localize the RAB11-UNC13D-FAK axis inside pancreatic cancer cells, we conducted immunofluorescence experiments. The results showed colocalization of UNC13D with FAK and RAB11 in recycling endosomes from the cell periphery to the perinuclear region (Fig. 3G).

Next, to determine whether the interaction between RAB11 and FAK affects the phosphorylation of FAK and its downstream signaling, we knocked down RAB11 in PANC-1 cells. Accordingly, siRAB11 reduced the phosphorylation of FAK and PXN (Fig. 3H).

Previous research has demonstrated that active β 1-integrins have a greater rate of endocytosis than inactive β 1-integrins [29]. While inactive β 1-integrins recycle through RAB4-dependent pathways, active β 1-integrins recycle mostly through RAB11-dependent pathways [29, 30]. To examine whether the recycling of ITGB1 is coupled to the RAB11-UNC13D axis, we performed immunofluorescence experiments. The active β 1 integrin was assessed by immunofluorescent staining using an antibody that specifically recognizes the active conformation (clone 12G10 anti-ITGB1). The co-localization of ITGB1 with FAK, RAB11 and UNC13D was observed in PANC-1 cells (Fig. 3G, Supplementary Fig. 4).

UNC13D directly interacts with FAK via the FERM domain in a calcium-dependent manner

Next, we attempted to map the peptide domain involved in the UNC13D/FAK interaction. Co-immunoprecipitation experiments were performed to map the interaction domains between UNC13D and different domains of FAK (N-terminal FERM domain, amino acids 1–423; KINASE domain, amino acids 416–680; C-terminal FAT domain, amino acids 677–1052). As shown in Fig. 4A, UNC13D interacts with the FERM domain of FAK. The crystal structure of FAK revealed an autoinhibitory conformation of the FERM-kinase region; FAK became auto-phosphorylated at Tyr397 after interactions between the FERM and kinase domains were released [31]. This suggests that UNC13D binds directly to the FERM domain, which promotes FAK activation.

To identify the UNC13D domains required for FAK activation, we constructed a series of UNC13D

(See figure on next page.)

Fig. 3 RAB11-UNC13D-FAK axis in recycling endosomes regulates the phosphorylation of FAK. **A** UNC13D knockdown in CAPAN-1 and PANC-1 cells decreased FAK/PXN signaling, which was measured by p-FAK, p-PXN, FAK, and PXN. Data are presented as the mean \pm SD. The experiments were independently performed at least three times. Statistical analysis was performed using Student's unpaired T test. $**p < 0.01$, $***p < 0.001$. **B** Co-immunoprecipitation analysis of the binding between exogenous Flag-UNC13D and HA-FAK in co-transfected HEK293 cells indicates the direct interaction of them. IgG was incubated with cell lysates as negative controls. **C** Immunoprecipitation of endogenous FAK from CAPAN-1 and PANC-1 cells confirms the binding between endogenous UNC13D and FAK. **D** Immunoprecipitation of endogenous RAB11 from PANC-1 overexpressing Flag-UNC13D cells indicates the binding between UNC13D and endogenous RAB11. **E** Co-immunoprecipitation analysis of the binding among RAB11, UNC13D, and FAK indicates the formation of RAB11-UNC13D-FAK complex. **F** UNC13D knockdown decreased the binding of RAB11 with FAK. RAB11 was immunoprecipitated from PANC-1 expressing shUNC13D or shSCR to examine the dependency of the interaction between RAB11 and FAK on UNC13D. **G** Co-localization of FAK, UNC13D, ITGB1, and RAB11 in PANC-1 cells. GFP-FAK, mOrange-UNC13D, and mCerulean-Rab11A cells were transduced. For the active integrin staining, 12G10 anti-ITGB1 was used. The data shown are representative of three independent experiments. Scale bar: 10 μ m. **H** RAB11A knockdown in CAPAN-1 and PANC-1 cells decreased FAK/PXN signaling, which was measured by pFAK, pPaxillin (p-PXN), FAK, and Paxillin (PXN). The quantification of western blotting in **(G)** is presented as the mean \pm SD of three independent experiments. Student's unpaired T test, $**p < 0.01$, $***p < 0.001$, $****p < 0.0001$

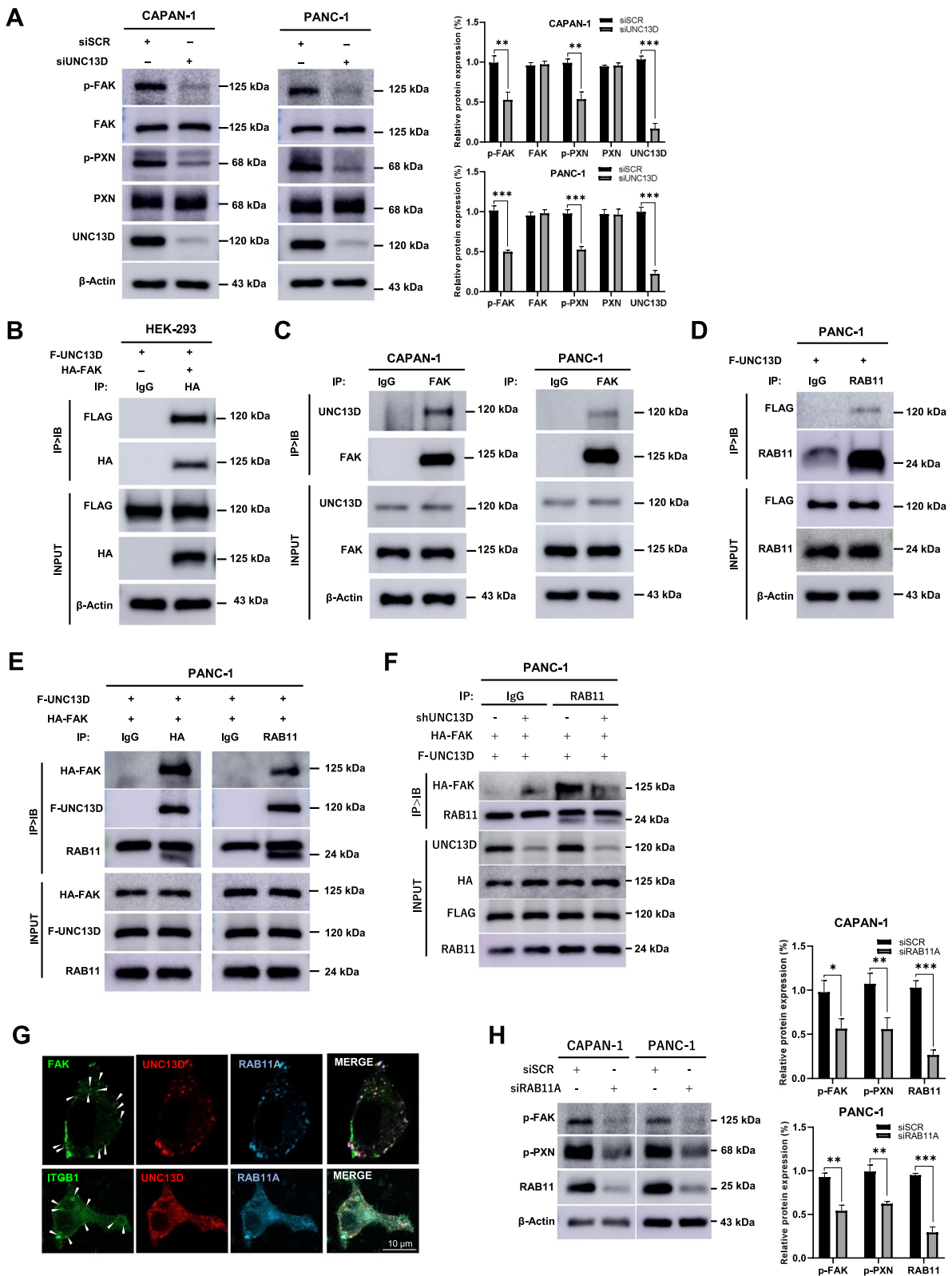


Fig. 3 (See legend on previous page.)

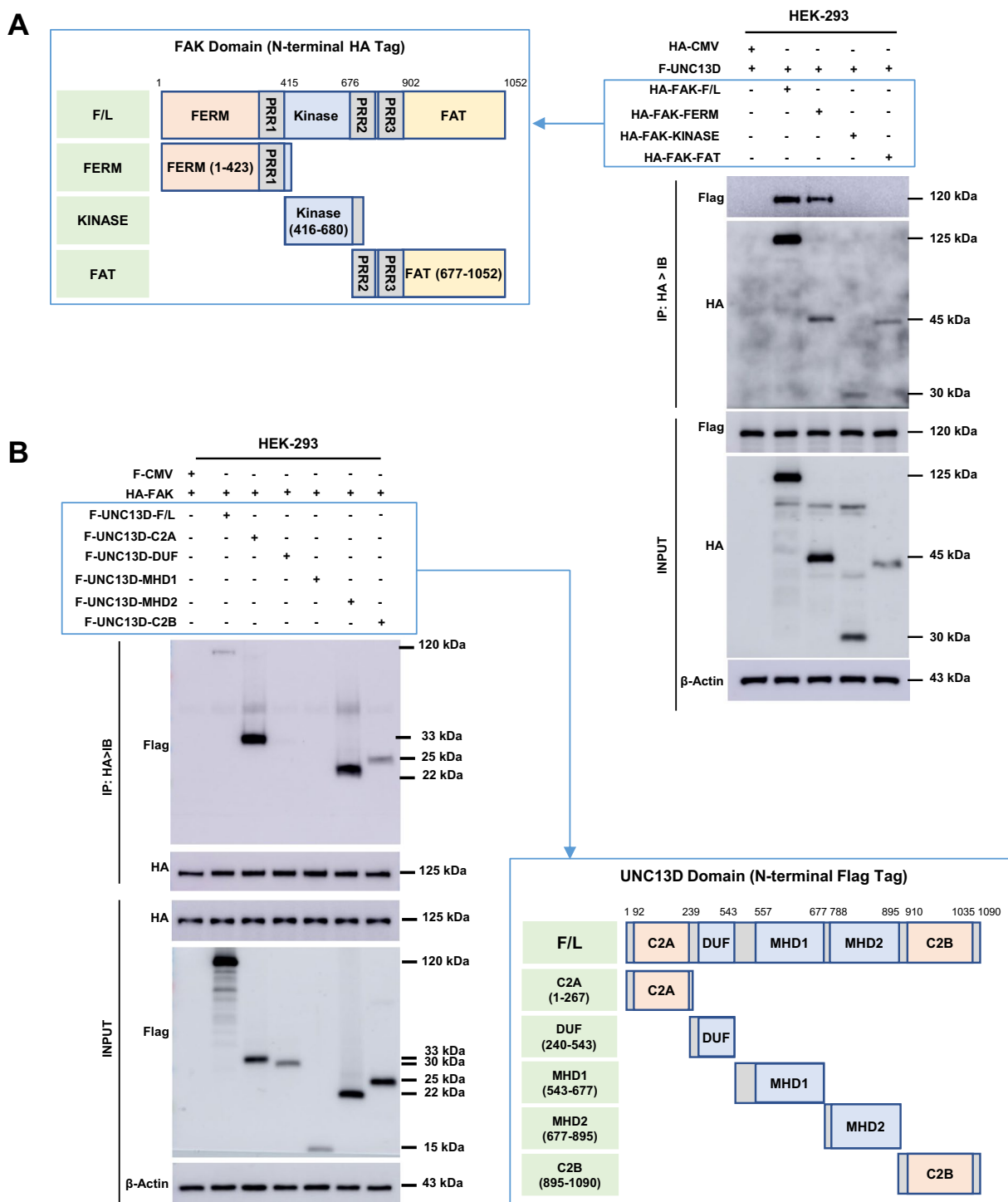


Fig. 4 Analysis of the interaction domains of FAK and UNC13D. **A** Co-immunoprecipitation assay after the transduction of full-length FAK or its truncation mutants in HEK293 cells. Each group was purified by immunoprecipitation with HA beads, followed by a western blot to detect FLAG-UNC13D with the anti-FLAG antibody. **B** Co-immunoprecipitation analysis after transduction of full-length UNC13D or its truncation mutants in HEK293 cells. Each group was purified by immunoprecipitation with HA beads, followed by a western blot to detect FLAG-UNC13D with the anti-FLAG antibody

truncation mutants (C2A domain, amino acids 1–267; DUF domain, amino acids 240–543; MHD1 domain, amino acids 543–677; MHD2 domain, amino acids 677–895; and C2B domain, amino acids 895–1090) (Fig. 4B). Co-immunoprecipitation results showed that FAK directly interacted with both the C2 domain and MHD2 of UNC13D (Fig. 4B).

Previous studies have revealed that UNC13D is a tethering or priming factor that functions as a Ca^{2+} sensor for both heterotypic secretory granule (SG)—plasma membrane and homotypic SG-SG fusion. To assess whether UNC13D functions as a potential Ca^{2+} sensor in pancreatic cancer cells, we examined the effects of calcium concentrations using a calcium ionophore (ionomycin) and a calcium chelator (EGTA). We observed that ionomycin-induced Ca^{2+} elevation was sufficient to enhance the phosphorylation of FAK, SRC, PXN, and ERK1/2. In contrast, Ca^{2+} captured by EGTA exhibited the opposite effect (Fig. 5A).

To determine whether the interaction between UNC13D and FAK was calcium-dependent, we co-expressed FLAG-UNC13D and HA-FAK in HEK293 cells and then treated the cells with ionomycin and EGTA. The co-immunoprecipitation results showed that the chelation of Ca^{2+} by EGTA decreased the interaction of UNC13D-FAK (Fig. 5B). Although its effect was not statistically significant, there was a tendency that the ionomycin treatment increased the interaction (Fig. 5B).

To further investigate calcium dependency during UNC13D binding-induced activation of FAK, we examined the effects of mutations in the calcium-binding domains of UNC13D. Specifically, two aspartate residues were mutated to asparagine in either the C2A (D127N and D133N) or C2B (D941N and D947N) domains, as well as a combination of both (D127N, D133N, D941N, and D947N). These proteins were termed C2A*

UNC13D, C2B* UNC13D, and C2A*B* UNC13D. The individual mutation of the UNC13D sequence in C2A* or C2B* did not impair the UNC13D-FAK interaction. However, the combined mutation of C2A* and C2B* dramatically impaired it (Fig. 5C). These results show that both the C2A and C2B domains are required for the interaction between UNC13D and FAK.

Prognostic significance of FAK (PTK2) in pancreatic cancer patients

Finally, we examined whether FAK expression is associated with patient prognosis. Kaplan–Meier curve analysis for survival with respect to FAK (PTK2) gene expression in four independent cohorts (TCGA, $n=178$; ICGC, $n=91$; GSE21501, $n=102$; and GSE28735, $n=45$) showed that its expression was associated with shorter survival rates in TCGA and GSE28735 cohorts ($p=0.005$, $p=0.007$, respectively; Fig. 1E). Moreover, co-expression of UNC13D and FAK showed the poorest prognosis in TCGA, ICGC, and GSE28735 cohorts ($p=0.000$, $p=0.036$, $p=0.006$, respectively; Fig. 1E). Furthermore, univariate analysis showed significance in three cohorts (TCGA, $p=0.006$, HR=2.299; ICGC, $p=0.012$, HR=2.043; GSE28735, $p=0.014$, HR=2.890, Table 2) although there is no association with clinicopathological characteristics (Supplementary Table 1). Multivariate analysis also showed a consistent result in TCGA cohort ($p=0.003$, HR=2.487, Table 2).

Discussion

Extensive efforts have been made to develop new biomarkers for pancreatic cancer. In addition to CA19-9 [32], methylation of the MUC1/4 gene [33], BRCA mutational status [34], and the expression of SPARC [35] and RAB27 [36] have been suggested as good prognostic markers. The level of the glypican-1 (GPC1) endosomes

(See figure on next page.)

Fig. 5 The interaction of UNC13D with FAK is calcium-dependent. **A** The modulation of calcium-regulated FAK/PXN signaling was measured by the expression level of p-FAK, p-SRC, p-PXN, and p-ERK. The level of calcium was modulated by the treatment with ionomycin 1.25 μM or EGTA 1 mM for 5 min. **B** The interaction of UNC13D with FAK is modulated by the calcium. The binding between UNC13D and FAK in HEK293 cells was examined by immunoprecipitation after the modulation of calcium concentration by ionomycin 1.25 μM or EGTA 1 mM for 5 min. The quantification data were shown as mean \pm SD of three independent experiments. Statistical significance was calculated using a one-way ANOVA with Tukey's multiple comparison test. * p value < 0.001 **(C)** Mutations of calcium-binding domains (C2A or C2B) in UNC13D regulated its interaction with FAK. UNC13D wild type or C2 mutants (C2A or C2B) in HEK293 cells were immunoprecipitated with HA beads and immunoblotted by anti-FLAG antibody for the detection of Flag-UNC13D. The quantification data were shown as mean \pm SD of three independent experiments. Statistical significance was calculated using a one-way ANOVA with Tukey's multiple comparison test. ** p value < 0.001 **(D)** The abstract figure indicating recycling machinery of integrin coupled with FA turnover via RAB11-UNC13D-FAK axis for migration of pancreatic cancer cells. Continuous recycling of integrin via exocytosis and endocytosis of vesicles is required for migration of cancer cells. Through exocytosis of endosomal vesicles, endocytosed integrin reaches at the plasma membrane of leading edge. During the assembly of FA, integrins interact with the extracellular matrix and recruit many proteins including talin, vinculin, paxillin and FAK. During the disassembly of FA, FA complex proteins are disintegrated and integrin is endocytosed into endosomal vesicles in a FAK-dependent manner. During the recycling process of integrin, UNC13D plays roles in tethering and priming of endosomal vesicles to the plasma membrane. Moreover, it can regulate disassembly of FA via RAB11-UNC13D-FAK axis. UNC13D knockdown inhibits exocytosis of endosomal vesicles and disassembly of FA, and finally cellular migration

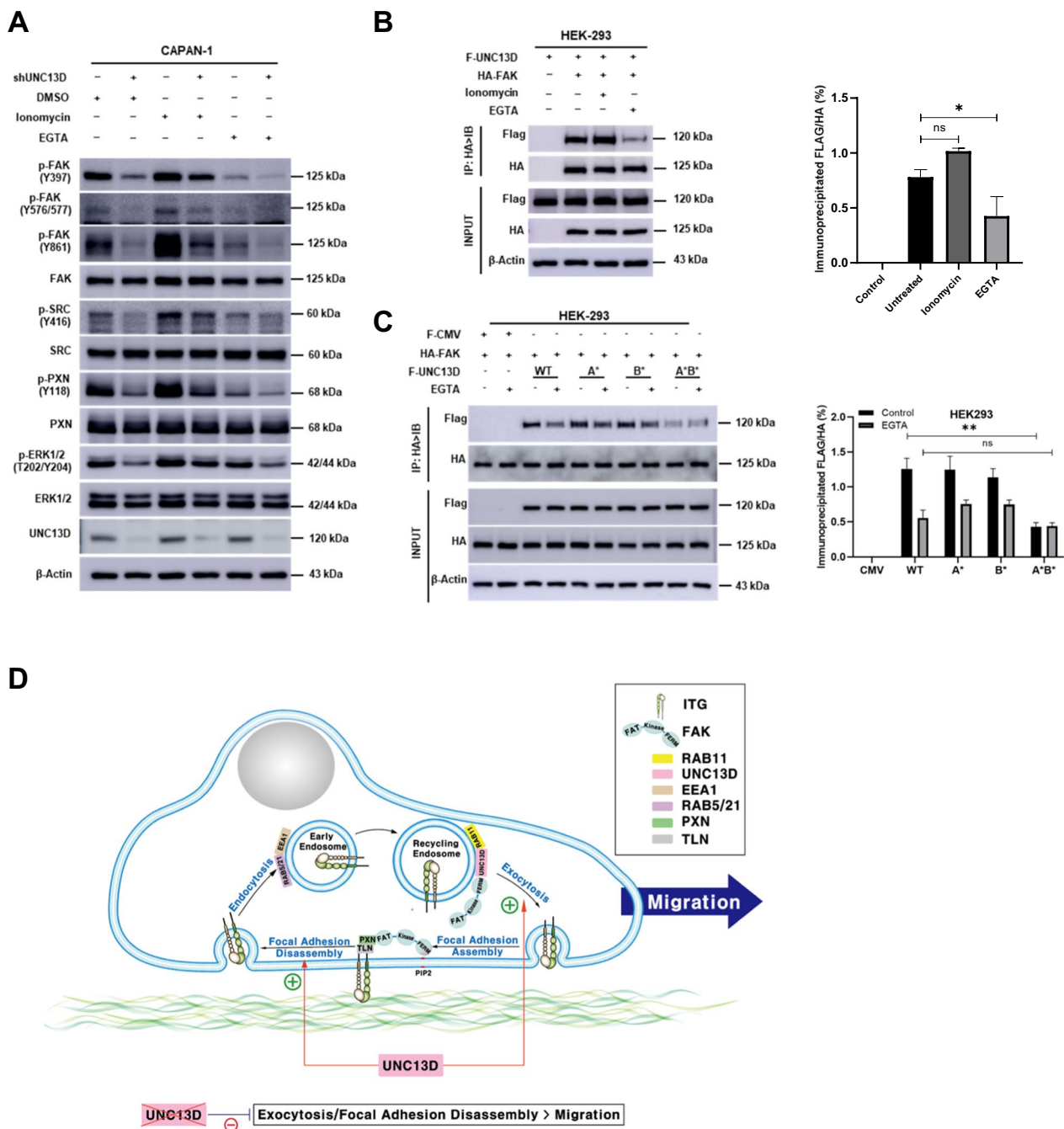


Fig. 5 (See legend on previous page.)

has also been shown to be a good prognostic marker in patients with pancreatic cancer. In this study, the clinical significance of UNC13D as a prognostic factor of pancreatic cancer was demonstrated in four independent cohorts (Fig. 1). Its efficacy as a biomarker was validated (Fig. 1). Moreover, the multivariate analysis proved to be a significant factor (Table 2).

Metastasis of cancer cell is a critical cause of cancer deaths. Median survival for patients with metastatic pancreatic cancer remains less than 1 year [37]. So, the migrastatic therapy may improve the survival of patients because they can reduce the need for high-dose cytotoxic therapies and show a synergistic effect [38]. Moreover, it may not cause resistance to conventional therapies based on anti-proliferative effects because targeted mechanisms

are quite different. Molecular targets for the migrastatic therapy include ATP availability, mitochondrial metabolism, cytoskeletal dynamics and cell contractility. The present study showed that siUNC13D can inhibit the migration and invasion of pancreatic cancer cells via the regulation of endosomal traffic, suggesting it can be a good molecular target for the migrastatic therapy.

Endosomes are an important signaling platform for integrin and growth factor receptors. A previous study has shown that FAK localizes with active integrins during endocytosis [2]. The endocytosis of integrins activates FAK in Rab21 dependent manner and prevents anoikis in cancer cells. However, how FAK is recruited to the endosome or how FAK activity is maintained in the active state is not well understood because active or inactive integrins can bind to endosomes [2]. Chen et al. showed a possible scenario in which co-endocytosed c-Met directly binds to FAK and phosphorylates it [39]. Another possible scenario is that integrin ligands, including collagen, fibronectin, and talin, inside early endosomes activate FAK [2]. However, the FAT domain of FAK does not localize to endosomes, suggesting that different mechanisms underlie FAK recruitment to FAs or endosomes. Another possible mechanism involves the interaction of FAK with PI (3,4,5)P in the endosomal membrane. A mass spectrometry-based study showed that FAK interact with PI3P [40]. In this study, we demonstrated that UNC13D is a key molecule involved in the recruitment of FAK to RAB11-positive recycling endosomes. Immunoprecipitation showed a direct interaction between UNC13D and FAK (Fig. 3), and immune-cytochemistry confirmed the co-localization of UNC13D and FAK in RAB11-positive recycling endosomes (Fig. 3). This direct interaction with FAK increases its phosphorylation status and the turnover of FAs (Fig. 2).

Endosomal signaling of FAK is strictly dependent on its tyrosine kinase activity, whereas conformational activation is dispensable for vesicular targeting. Several studies have documented that the FERM domain is adequate for recruiting FAK to endosomes containing active integrins; however, the specific mechanisms driving this process remain unknown [29, 30, 41]. It has been firmly established that the MHD region facilitates the localization of UNC13D on RAB11-associated recycling endosomes [42]. Our data suggest that UNC13D functions as a scaffold protein in the endosome, coordinating the recruitment and activation of FAK through its FERM domain, and that this mechanism is dependent on RAB11. Previous studies have reported that phosphorylated FAK is observed not only within FAs but also on endosomes in adherent cells, and active integrin and FAK signaling localized in

endosomes plays a role in cancer-related processes, such as anchorage-independent growth and metastasis [2]. In this study, we showed that the knockdown of RAB11 and UNC13D reduced FAK phosphorylation (Fig. 3), suggesting that the RAB11-UNC13D-FAK axis is critical for the maintenance of FAK signaling.

There is controversy regarding direct interactions between RAB11 and UNC13D. Menaget et al. did not find a direct interaction between RAB11 and UNC13D, although they co-localized in endosomes [42]. However, a later study showed that UNC13D binds to RAB11, and UNC13D-deficient neutrophils retain RAB11-positive vesicles in the plasma membrane [4]. In this study, we demonstrated the direct interaction of UNC13D with RAB11 and their co-localization in endosomes (Fig. 3).

UNC13D, a 120-kDa protein (also known as Munc13-4), belongs to the Munc13 (mammalian homolog of the *Caenorhabditis elegans* uncoordinated gene 13) family, which is highly expressed in hematopoietic cells as well as in the lungs, kidneys, and other organs with secretory functions. UNC13D contains N- and C-terminal Ca²⁺-binding C2 domains, two Munc-homology domains (MHD), and a non-canonical Rab27a-binding motif in the N-terminus of UNC13D corresponds to amino acids 240–543 [43, 44]. UNC13D C2 domains specifically bind calcium, regulate exocytosis in a calcium- and SNARE-dependent manner, and interact with phospholipids via their C2 domains [45, 46]. C2 domains, together with MHD domains, are critical for the tethering or priming of vesicles via binding to membrane phospholipids or the SNARE complex [46]. In this study, we observed that the UNC13D domains were also critical for binding to the FERM domain of FAK (Figs. 4, 5). These data, together with previous reports, suggest that binding is transient and possibly occurs before tethering or priming of endosomal vesicles.

FAK is critical for FA disassembly [41, 47–49]. The localization of FAK is in an equilibrium state between FAs and the cytosol. A previous study showed that phosphorylation of FAK increased the residence time of FAK at FAs. In this study, we show that RAB11 and UNC13D regulate FAK phosphorylation, which can lead to changes in FA turnover (Figs. 2, 3). Collectively, these results suggest that FAK phosphorylation at recycling endosomes favors the equilibrium of FAK with FAs.

Due to its critical roles in the progression of cancer, many drugs targeting FAK are under clinical trials [10]. Notably the connection between FAK and drug resistance has been reported. The usefulness of FAK inhibition to overcome the resistance to chemotherapies including KRAS inhibitors, osimertinib, platinum, and doxorubicin was demonstrated in various cancer types [50–53]. In addition, the combination of FAK and ROS1 inhibitors

showed a synergism in triple-negative breast cancer and CDH1-deficient cancers [54, 55]. In pancreatic cancer FAK inhibition increased radio-sensitivity of cancer cells [56, 57]. In the present study we showed the prognostic significance of FAK in the pancreatic cancer (Table 2), the poorest prognosis in the UNC13D-high and FAK-high group (Fig. 1E), and the UNC13D-FAK axis for the migration of pancreatic cancer cells. So, various kinds of combination treatments need to be examined in the future study.

Conclusions

In summary, we observed that the RAB11-UNC13D-FAK axis couples exocytosis of endosomes with the turnover of FAs, which regulates the migration of pancreatic cancer cells (Fig. 5D). The direct calcium-dependent interaction between UNC13D and the FAK FERM domain is critical for the regulation of FAK phosphorylation. We also observed that the key molecule, UNC13D, for this coupling, is a novel prognostic factor for patients with pancreatic cancer, which was confirmed in four independent cohorts.

Abbreviations

C2 Domain	Protein kinase C conserved region 2/Calcium-binding motif
DAPI	4',6-Diamidino-2-phenylindole
DMSO	Dimethyl sulfoxide
DUF	Domain of unknown function
EEA1	Early endosome antigen 1
EGTA	Ethylene glycol-bis-(beta-aminoethyl ether)-N,N,N',N'-tetraacetic acid
Erk	Extracellular signal-regulated kinase
FA	Focal adhesion
FAT	Focal adhesion targeting
FERM	Protein 4.1, ezrin, radixin, moesin
F/L	Full length
F-UNC13D	Flag-UNC13D
FAK	Focal adhesion kinase
GENT	Gene Expression database of Normal and Tumor tissues
GEO	Gene Expression Omnibus
GS	Secretory granule
GSE	GEO data series
GTEX	Genotype-Tissue Expression
HA	Hemagglutinin
ICGC	International Cancer Genome Consortium
IB	Immunoblotting
IP	Immunoprecipitation
ITGB1	Integrin beta1
MHD	Munc homology domain
NDZ	Nocodazole
PC	Pancreatic cancer
PCR	Polymerase chain reaction
PXN	Paxillin
Rab11	Ras-related protein Rab-11
shRNA	Short hairpin RNA
siRNA	Small interfering RNA
Src	Proto-oncogene tyrosine-protein kinase
TCGA	The Cancer Genome Atlas
TLN	Talin1
UNC13D	Unc-13 homolog D
Y	Tyrosine

Supplementary Information

The online version contains supplementary material available at <https://doi.org/10.1186/s12967-024-05630-9>.

Supplementary Material 1: Fig. 1. Boyden chamber assay of cell migration capacity upon UNC13D knockdown in CAPAN-1 and SNU213 cells. Data are presented as the mean±SD. Two-tailed unpaired Student T test, ***p* < 0.01. The assay was performed 48h after the transfection with scrRNA or siUNC13D. The quantification data shown are representative of three independent experiments.

Supplementary Material 2: Fig. 2. Immunofluorescence analysis of FA in pancreatic cancer cells. CAPAN-1 shSCR or shUNC13D cells were fixed and immunostained with anti-PXN and anti-F-actin antibodies. PXN in green, and F-actin in red. Scale bar, 10 μm.

Supplementary Material 3: Fig. 3. VS4718, a FAK inhibitor, reduced UNC13D-induced cell migration. A-C, HEK293 cells were transfected with the indicated plasmids, treated with or without FAK inhibitor and then were harvested for immunoblotting analysis. B and C, Representative images and the corresponding quantification of Boyden transwell assay of HEK293 cells treated as indicated in. D-F, PANC-1 cells were transfected with the indicated plasmids, treated with or without FAK inhibitor and then were harvested for immunoblotting analysis. E and F, Representative images and the corresponding quantification of Boyden transwell assay of PANC-1 cells treated as indicated in. Data were shown as mean±SD of three independent experiments. Statistical significance was calculated using a one-way ANOVA with Tukey's multiple comparison test. * *p* value < 0.05, ** *p* value < 0.01, *** *p* value < 0.001. Scale bar, 200 μm.

Supplementary Material 4: Fig. 4. Co-localization of p-FAK with active integrin in pancreatic cancer cells. CAPAN-1 cells were fixed and immunostained with anti-phospho-FAK and anti-active integrin antibodies. P-FAK-Y397 in green, and active integrin red. Ort Sec: orthogonal section. The data shown are representative of three independent experiments. Scale bar, 10 μm.

Supplementary Material 5: Table 1. Clinicopathological characteristics of patients and their association with FAK expression.

Supplementary Material 6: Table 2. List of primers, primary antibodies and reagents.

Acknowledgements

The pcDNA3.1-FAK-HA and pcDNA3.1-FAK-HA domain plasmids were kindly provided by Prof. Min Do Sik (Department of Pharmacy, Yonsei University, Korea).

Author contributions

Writing (original draft) by VT Duong, public data base investigation and formal analysis by M Ha and ME Han, biological experiments by VT Duong, Jayoung Kim, Siyoung Park, Khatun Mst Reshma, and Ji-Young Kim, conceptualization, supervision and writing by D Lee, Y Kim, SO Oh.

Funding

This work was supported by grants from the Medical Research Center (MRC) Program (NRF-2022R1A5A2027161) and from the Mid-career Research Grant (NRF-2022R1A2C1003930) of the National Research Foundation (NRF) funded by the Korean government (MSIT). The funders had no role in study design, data collection and analysis, decision to publish, or preparation of the manuscript.

Availability of data and materials

Derived data supporting the findings of this study and materials are available from the corresponding author [SO Oh] on request.

Declarations

Ethics approval and consent to participate

There was no patient participation or animal experiment for this manuscript.

Consent for publication

The manuscript has been read and approved by all the listed authors.

Competing interests

The authors declare no potential conflicts of interest.

Author details

¹Department of Anatomy, School of Medicine, Pusan National University, Yangsan, Republic of Korea. ²Department of Nuclear Medicine and Medical Research Institute, School of Medicine, Pusan National University, Yangsan, Republic of Korea. ³Department of Convergence Medicine, School of Medicine, Pusan National University, Yangsan, Republic of Korea. ⁴Department of Biomedical Informatics, School of Medicine, Pusan National University, Yangsan, Republic of Korea.

Received: 11 May 2024 Accepted: 18 August 2024

Published online: 29 August 2024

References

- Wilson BJ, Allen JL, Caswell PT. Vesicle trafficking pathways that direct cell migration in 3D matrices and in vivo. *Traffic*. 2018;19(12):899–909.
- Alanko J, Mai A, Jacquemet G, Schauer K, Kaukonen R, Saari M, Goud B, Ivaska J. Integrin endosomal signalling suppresses anoikis. *Nat Cell Biol*. 2015;17(11):1412–21.
- Danen EHJ, van Rheenen J, Franken W, Huvencuers S, Sonneveld P, Jalink K, Sonnenberg A. Integrins control motile strategy through a Rho-cofilin pathway. *J Cell Biol*. 2005;169(3):515–26.
- Johnson JL, He J, Ramadass M, Pestonjamas P, Kiosses WB, Zhang JZ, Catz SD. Munc13-4 is a Rab11-binding protein that regulates Rab11-positive vesicle trafficking and docking at the plasma membrane. *J Biol Chem*. 2016;291(7):3423–38.
- van der Sluijs P, Zibouche M, van Kerkhof P. Late steps in secretory lysosome exocytosis in cytotoxic lymphocytes. *Front Immunol*. 2013;4:1–7.
- Messenger SW, Woo SS, Sun ZZ, Martin TFJ. A Ca²⁺/SUP>2+</SUP>-stimulated exosome release pathway in cancer cells is regulated by Munc13-4. *J Cell Biol*. 2018;217(8):2877–90.
- Nagano M, Hoshino D, Koshikawa N, Akizawa T, Seiki M. Turnover of focal adhesions and cancer cell migration. *Int J Cell Biol*. 2012;2012:1–10.
- Zhao X, Guan JL. Focal adhesion kinase and its signaling pathways in cell migration and angiogenesis. *Adv Drug Deliver Rev*. 2011;63(8):610–5.
- Ezratty EJ, Partridge MA, Gundersen GG. Microtubule-induced focal adhesion disassembly is mediated by dynamin and focal adhesion kinase. *Nat Cell Biol*. 2005;7(6):581–90.
- Tan X, Yan Y, Song B, Zhu S, Mei Q, Wu K. Focal adhesion kinase: from biological functions to therapeutic strategies. *Exp Hematol Oncol*. 2023;12(1):1–19.
- Zhang L, Qu J, Qi Y, Duan Y, Huang YW, Zhou Z, Li P, Yao J, Huang B, Zhang S, et al. EZH2 engages TGFβ signaling to promote breast cancer bone metastasis via integrin β1-FAK activation. *Nat Commun*. 2022;13(1):1–16.
- Lim ST, Chen XL, Lim Y, Hanson DA, Vo TT, Howerton K, Larocque N, Fisher SJ, Schlaepfer DD, Ilic D. Nuclear FAK promotes cell proliferation and survival through FERM-enhanced p53 degradation. *Mol Cell*. 2008;29(1):9–22.
- Frame MC, Patel H, Serrels B, Lietha D, Eck MJ. The FERM domain: organizing the structure and function of FAK. *Nat Rev Mol Cell Biol*. 2010;11(11):802–14.
- Sieg DJ, Hauck CR, Ilic D, Klingbeil CK, Schaefer E, Damsky CH, Schlaepfer DD. FAK integrates growth-factor and integrin signals to promote cell migration. *Nat Cell Biol*. 2000;2(5):249–56.
- Chen TH, Chan PC, Chen CL, Chen HC. Phosphorylation of focal adhesion kinase on tyrosine 194 by Met leads to its activation through relief of autoinhibition. *Oncogene*. 2011;30(2):153–66.
- Schlaepfer DD, Hanks SK, Hunter T, van der Geer P. Integrin-mediated signal transduction linked to Ras pathway by GRB2 binding to focal adhesion kinase. *Nature*. 1994;372(6508):786–91.
- Webb DJ, Donais K, Whitmore LA, Thomas SM, Turner CE, Parsons JT, Horwitz AF. FAK-Src signalling through paxillin, ERK and MLCK regulates adhesion disassembly. *Nat Cell Biol*. 2004;6(2):154–61.
- Ren XD, Kiosses WB, Sieg DJ, Otey CA, Schlaepfer DD, Schwartz MA. Focal adhesion kinase suppresses Rho activity to promote focal adhesion turnover. *J Cell Sci*. 2000;113(Pt 20):3673–8.
- Schober M, Raghavan S, Nikolova M, Polak L, Pasolli HA, Beggs HE, Reichardt LF, Fuchs E. Focal adhesion kinase modulates tension signaling to control actin and focal adhesion dynamics. *J Cell Biol*. 2007;176(5):667–80.
- Siegel RL, Miller KD, Wagle NS, Jemal A. Cancer statistics, 2023. *Ca-Cancer J Clin*. 2023;73(1):17–48.
- Neoptolemos JP, Kleeff J, Michl P, Costello E, Greenhalf W, Palmer DH. Therapeutic developments in pancreatic cancer: current and future perspectives. *Nat Rev Gastro Hepat*. 2018;15(6):332–47.
- Jeon TY, Han ME, Lee YW, Lee YS, Kim GH, Song GA, Hur GY, Kim JY, Kim HJ, Yoon S, et al. Overexpression of stathmin1 in the diffuse type of gastric cancer and its roles in proliferation and migration of gastric cancer cells. *Brit J Cancer*. 2010;102(4):710–8.
- Tran MT, Okusha Y, Feng YX, Sogawa C, Eguchi T, Kadowaki T, Sakai E, Tsukuba T, Okamoto K. A novel role of HSP90 in regulating osteoclastogenesis by abrogating Rab11b-driven transport. *Bba-Mol Cell Res*. 2021;1868(10):1–14.
- Webb DJ, Parsons JT, Horwitz AF. Adhesion assembly, disassembly and turnover in migrating cells - over and over and over again. *Nat Cell Biol*. 2002;4(4):E97–100.
- Wu SY, Chen M, Huang J, Zhang FF, Lv ZJ, Jia YX, Cui YZ, Sun LZ, Wang Y, Tang Y, et al. ORAI2 promotes gastric cancer tumorigenicity and metastasis through PI3K/Akt Signaling and MAPK-dependent focal adhesion disassembly. *Cancer Res*. 2021;81(4):986–1000.
- Hamidi H, Ivaska J. Every step of the way: integrins in cancer progression and metastasis. *Nat Rev Cancer*. 2018;18(9):532–47.
- Mitra SK, Hanson DA, Schlaepfer DD. Focal adhesion kinase: In command and control of cell motility. *Nat Rev Mol Cell Bio*. 2005;6(1):56–68.
- Fletcher SJ, Rappoport JZ. Moving forward: polarised trafficking in cell migration. *Trends Cell Biol*. 2010;20(2):71–8.
- Arjonen A, Alanko J, Veltel S, Ivaska J. Distinct recycling of active and inactive β1 integrins. *Traffic*. 2012;13(4):610–25.
- Mana G, Valdembrì D, Serini G. Conformationally active integrin endocytosis and traffic: why, where, when and how? *Biochem Soc T*. 2020;48(1):83–93.
- Lietha D, Cai XM, Ceccarelli DFJ, Li YQ, Schaller MD, Eck MJ. Structural basis for the autoinhibition of focal adhesion kinase. *Cell*. 2007;129(6):1177–87.
- Poruk KE, Gay DZ, Brown K, Mulvihill JD, Boucher KM, Scaife CL, Firpo MA, Mulvihill SJ. The clinical utility of CA 19–9 in pancreatic adenocarcinoma: diagnostic and prognostic updates. *Curr Mol Med*. 2013;13(3):340–51.
- Yokoyama S, Higashi M, Kitamoto S, Oeldorf M, Knippschild U, Kornmann M, Maemura K, Kurahara H, Wiest E, Hamada T, et al. Aberrant methylation of MUC1 and MUC4 promoters are potential prognostic biomarkers for pancreatic ductal adenocarcinomas. *Oncotarget*. 2016;7(27):42553–65.
- Zhu Y, Zhai K, Ke J, Li J, Gong Y, Yang Y, Tian J, Zhang Y, Zou D, Peng X, et al. BRCA1 missense polymorphisms are associated with poor prognosis of pancreatic cancer patients in a Chinese population. *Oncotarget*. 2017;8(22):36033–9.
- Miyoshi K, Sato N, Ohuchida K, Mizumoto K, Tanaka M. SPARC mRNA expression as a prognostic marker for pancreatic adenocarcinoma patients. *Anticancer Res*. 2010;30(3):867–71.
- Wang Q, Ni Q, Wang X, Zhu H, Wang Z, Huang J. High expression of RAB27A and TP53 in pancreatic cancer predicts poor survival. *Med Oncol*. 2015;32(1):372.
- Gyawali B, Booth CM. Treatment of metastatic pancreatic cancer: 25 years of innovation with little progress for patients. *Lancet Oncol*. 2024;25(2):167–70.
- Raudenska M, Petrlikova K, Jurinakova T, Leischner Fialova J, Fojtu M, Jakubek M, Rosel D, Brabek J, Masarik M. Engine shutdown: migrastatic strategies and prevention of metastases. *Trends Cancer*. 2023;9(4):293–308.
- Chen SY, Chen HC. Direct interaction of focal adhesion kinase (FAK) with Met is required for FAK to promote hepatocyte growth factor-induced cell invasion. *Mol Cell Biol*. 2006;26(13):5155–67.

40. Catimel B, Kapp E, Yin MX, Gregory M, Wong LSM, Condrón M, Church N, Kershaw N, Holmes AB, Burgess AW. The PI(3)P interactome from a colon cancer cell. *J Proteomics*. 2013;82:35–51.
41. Nader GPF, Ezratty EJ, Gundersen GG. FAK, talin and PIPKly regulate endocytosed integrin activation to polarize focal adhesion assembly. *Nat Cell Biol*. 2016;18(5):491–503.
42. Ménager MM, Ménasché G, Romão M, Knapnougel P, Ho CH, Garfa M, Raposo G, Feldmann J, Fischer A, Basile GD. Secretory cytotoxic granule maturation and exocytosis require the effector protein hMunc13-4. *Nat Immunol*. 2007;8(3):257–67.
43. Koch H, Hofmann K, Brose N. Definition of Munc13-homology-domains and characterization of a novel ubiquitously expressed Munc13 isoform. *Biochem J*. 2000;349:247–53.
44. Ramadass M, Catz SD. Molecular mechanisms regulating secretory organelles and endosomes in neutrophils and their implications for inflammation. *Immunol Rev*. 2016;273(1):249–65.
45. Boswell KL, James DJ, Esquibel JM, Bruinsma S, Shirakawa R, Horiuchi H, Martin TFJ. Munc13-4 reconstitutes calcium-dependent SNARE-mediated membrane fusion. *J Cell Biol*. 2012;197(2):301–12.
46. Pivot-Pajot C, Varoquaux F, de Saint BG, Bourgoïn SG. Munc13-4 regulates granule secretion in human neutrophils. *J Immunol*. 2008;180(10):6786–97.
47. He ZW, Wang J, Xu J, Jiang XY, Liu XY, Jiang JX. Dynamic regulation of KIF15 phosphorylation and acetylation promotes focal adhesions disassembly in pancreatic cancer. *Cell Death Dis*. 2022;13(10):1–13.
48. Klímová Z, Bráborec V, Maninová M, Cáslavský J, Weber MJ, Vomastek T. Symmetry breaking in spreading RAT2 fibroblasts requires the MAPK/ERK pathway scaffold RACK1 that integrates FAK, p190A-RhoGAP and ERK2 signaling. *Bba-Mol Cell Res*. 2016;1863(9):2189–200.
49. Wong BS, Shea DJ, Mistriotis P, Tuntithavornwat S, Law RA, Bieber JM, Zheng L, Konstantopoulos K. A direct podocalyxin-dynamin-2 interaction regulates cytoskeletal dynamics to promote migration and metastasis in pancreatic cancer cells. *Cancer Res*. 2019;79(11):2878–91.
50. Zhang B, Zhang Y, Zhang J, Liu P, Jiao B, Wang Z, Ren R. Focal Adhesion Kinase (FAK) Inhibition Synergizes with KRAS G12C Inhibitors in treating cancer through the Regulation of the FAK-YAP Signaling. *Adv Sci (Weinh)*. 2021;8(16):1–15.
51. Ichihara E, Westover D, Meador CB, Yan Y, Bauer JA, Lu P, Ye F, Kulick A, de Stanchina E, McEwen R, et al. SFK/FAK signaling attenuates osimertinib efficacy in both drug-sensitive and drug-resistant models of EGFR-mutant lung cancer. *Cancer Res*. 2017;77(11):2990–3000.
52. Diaz Osterman CJ, Ozmadenci D, Kleinschmidt EG, Taylor KN, Barrie AM, Jiang S, Bean LM, Sulzmaier FJ, Jean C, Tancioni I, et al. FAK activity sustains intrinsic and acquired ovarian cancer resistance to platinum chemotherapy. *Elife*. 2019;8:1–34.
53. Saatci O, Kaymak A, Raza U, Ersan PG, Akbulut O, Banister CE, Sikirzhyski V, Tokat UM, Aykut G, Ansari SA, et al. Targeting lysyl oxidase (LOX) overcomes chemotherapy resistance in triple negative breast cancer. *Nat Commun*. 2020;11(1):1–17.
54. Tan X, Kong D, Tao Z, Cheng F, Zhang B, Wang Z, Mei Q, Chen C, Wu K. Simultaneous inhibition of FAK and ROS1 synergistically repressed triple-negative breast cancer by upregulating p53 signalling. *Biomark Res*. 2024;12(1):1–24.
55. Gao J, Yao Y, Liu C, Xie X, Li D, Liu P, Wang Z, Zhang B, Ren R. Synergism of FAK and ROS1 inhibitors in the treatment of CDH1-deficient cancers mediated by FAK-YAP signaling. *Int J Biol Sci*. 2023;19(9):2711–24.
56. Chen H, Tu W, Lu Y, Zhang Y, Xu Y, Chen X, Zhu M, Liu Y. Low-dose X-ray irradiation combined with FAK inhibitors improves the immune microenvironment and confers sensitivity to radiotherapy in pancreatic cancer. *Biomed Pharmacother*. 2022;151:1–10.
57. Osipov A, Blair AB, Liberto J, Wang J, Li K, Herbst B, Xu Y, Li S, Niu N, Rashid R, et al. Inhibition of focal adhesion kinase enhances antitumor response of radiation therapy in pancreatic cancer through CD8+ T cells. *Cancer Biol Med*. 2021;18(1):206–14.

Publisher's Note

Springer Nature remains neutral with regard to jurisdictional claims in published maps and institutional affiliations.